Evaluation of Simple Subgrid-Scale Models for the Numerical Simulation of Homogeneous Turbulence

Khoa T. Dang*
Office National d'Etudes et de Recherches Aérospatiales, Chatillon, France

Several subgrid-scale models are evaluated in a 16^3 large eddy simulation (16 discretization points in each space direction) of isotropic and anisotropic turbulence and will be used in a 64^3 numerical simulation of homogeneous turbulence submitted to two successive plane strains. An inexpensive numerical code, implemented on a parallel structure system, has been used with simple eddy-viscosity subgrid-scale models. Decaying isotropic turbulence has been simulated with a 16^3 version of the code. Comparisons with experiment show the necessity for the eddy viscosity to allow both a strong local energy transfer near the cutoff wave number and a time-dependent nonlocal transfer. In the case of homogeneous turbulence submitted to two successive plane strains, time evolutions of turbulence energy and anisotropy obtained with 64^3 full-turbulence simulations (FTS), 16^3 large eddy simulations (LES), and classical one-point closure models compare well with experiment. The reorientation process of the Reynolds stress tensor during and after the second deformation is well simulated. The reorientation process of the slow-pressure/strain tensor (not accessible by experiment) is also described: it shows, as proposed by some authors, that the quantity to be modeled is a combination of the dissipation and slow-pressure/strain tensors. Some numerical difficulties due to the presence of strong deformation rates are identified and minimized by a judicious choice of the initial geometry of the predistorted grid.

Nomenclature

b_{ij}	= anisotropy tensor, $=\langle u_i u_j\rangle/\langle u_k u_k\rangle - \delta_{ij}/3$
D	= constant strain rate
$E(k)$	= three-dimensional energy spectrum
$E_{ii}(k)$	= three-dimensional spectrum of $u_i(k)$
G	= anisotropy parameter, $1/9 + \mathrm{III} - \mathrm{II}/2$
$\boldsymbol{k}$	= wave number vector
k	= wave number
K	= anisotropy parameter, $=(u_{\mathrm{III}}^2 - u_{\mathrm{II}}^2)/(u_{\mathrm{III}}^2 + u_{\mathrm{II}}^2)$
$\langle (p^{(1)}/\rho) S_{ij}\rangle$	= slow-pressure/strain tensor
$\langle (p^{(2)}/\rho) S_{ij}\rangle$	= rapid-pressure/strain tensor
q^2	= turbulence energy, $\langle u_k u_k\rangle$
Re	= Reynolds number, $=q^{2^2}/9\nu\epsilon$
R_λ	= Reynolds number, $=\sqrt{q^2}\lambda/\nu$
S_{ij}	= strain rate tensor, $(u_{i,j} + u_{j,i})/2$
t	= time
$\bar{U}(x)$	= mean velocity vector
$\bar{U}_{i,j}$	= constant mean velocity gradient
$u(x)$	= fluctuating velocity vector
$\langle u_i u_j\rangle$	= Reynolds stress tensor
$\boldsymbol{x}$	= position vector
α	= angle between the two successive deformations
α_0	= angle defining the geometry of the initial predistorted computational grid
ϵ	= dissipation rate of turbulence energy, $=\nu\langle u_{i,k} u_{i,k}\rangle$
ϵ_{ij}	= dissipation tensor, $2\nu\langle u_{i,k} u_{j,k}\rangle$
λ	= Taylor microscale
ν	= molecular viscosity
ν_T	= eddy viscosity
II	= second invariant of the anisotropy tensor, $=b_{ij}b_{ji}$
III	= third invariant of the anisotropy tensor, $=b_{ik}b_{km}b_{mi}$

Presented as Paper 83-1692 at the AIAA 16th Fluid and Plasma Dynamics Conference, Danvers, Mass., July 12-14, 1983; received Aug. 23, 1983; revision received Feb. 29, 1984.

*Research Engineer, Aerodynamics Department.

I. Introduction

A. Numerical Code

A NUMERICAL code derived from the one proposed by Rogallo[15] has been achieved by Leca and Roy.[8] It allows homogeneous turbulence, submitted to a constant mean velocity gradient $\bar{U}_{i,j}$, to be simulated in a moving coordinate system (x_i') with periodic pseudospectral methods similar to those developed by Orszag and Patterson.[13] The moving frame is linearly related to a fixed, undistorted reference frame (x_i):

$$x_i' = B_{ij} x_j \tag{1}$$

Homogeneity is preserved[15,17] if

$$\dot{B}_{ij} = \bar{U}_{i,k} B_{kj} \tag{2}$$

Derivatives are computed in Fourier space (k_i), and products of two functions in physical space by multiplication. The second-order accurate time scheme is a quadrature for the diffusion term and a leap-frog scheme for convection.[17] Higher order schemes have been designed by Morchoisne[12] and Roy[18] but are not used because they require excessive computer resources.

Whereas Rogallo's code uses variables that are well adapted to the rapid distortion theory, the code presented herein works with the usual variables and is able to treat the most general distortion, i.e., superposition of rotation and strain with an arbitrary predistortion to avoid numerical difficulties.

A first version of this code was implemented on a parallel structure system including an array processor (AP 120 B) and a host (SEL 32/77). A multiprocessor version of this code is working now with two array processors. The computer time was reduced from 2 min 30 s (first version) to 56 s/time step[8]; this enables us to achieve numerical simulations at very low cost.

B. Treatment of Imposed Strains on Turbulent Flows

Homogeneous isotropic freely decaying turbulence has been simulated[17] with 64 points in each space direction at a Reynolds number of $R_\lambda \approx 60$ (based on Taylor microscale λ). However, the treatment of imposed strains on turbulent flows by the Lagrangian method leads to stretched computing domains and hence to a noticeable reduction of practical values of R_λ.

Therefore, some adequate subgrid-scale models are strongly needed to take into account the effect of the unresolved scales ($k > k_c$) on the resolved ones ($k \leq k_c$) when higher Reynolds number flows are to be simulated.

The parallel computing system has an attractive cost/performance ratio; however, this system also requires substantial programming work. In order to minimize the latter, simple subgrid models, which are based upon the eddy-viscosity hypothesis, are utilized for this initial study. It is recognized that this hypothesis and the LES modeling will not permit the existence of an energy transfer from the subgrid to the resolved scales. It is planned to study other models, such as those of Bardina et al.,[1] to overcome the deficiency of the present scheme.

Section II describes results obtained for isotropic turbulence with isotropic and anisotropic computational grids. Numerical difficulties arising from the use of stretched computational grids are noted.

Section III discusses results obtained for homogeneous turbulence submitted to two successive plane strains and their implications for turbulence modeling with one-point closures.

II. 16^3 Large Eddy Simulations of Isotropic Turbulence

A. "Isotropic" Computational Grid

The computations are done on a Cyber 170-750 in the case of a decaying isotropic turbulence with a 16^3 version of the code.

The computational grid has its points regularly spaced in a cubic box both in physical and spectral spaces. The filter used is of a top-hat type in spectral space, achieving a sharp low-pass cutoff at $k = k_c$ and eliminating the so-called Leonard stresses.[9]

The subgrid Reynolds stresses τ_{ij} are expressed by means of the resolved strain rate tensor S_{ij} and an eddy viscosity ν_T:

$$\tau_{ij} = -2\nu_T S_{ij} \tag{3}$$

where $S_{ij} = \frac{1}{2}(u_{i,j} + u_{j,i})$, $i,j = 1,2,3$.

Following general results obtained with two-point closures in spectral space,[3,10] ν_T is known to depend on the ratio k/k_c and the state of the turbulence. This can be expressed by means of a function $F(k/k_c)$ and an effective viscosity ν_e as follows:

$$\nu_T = \nu_e F(k/k_c) \tag{4}$$

Detailed expressions for ν_e and $F(k/k_c)$ are listed in Table 1.

The exponential dependence of

$$F(k/k_c) = 1 + \lambda (k/k_c)^{2(\alpha - 1)} \tag{5}$$

has been derived from a model proposed by Basdevant et al.[2] Their model was designed for two-dimensional simulations and insures an important local transfer of energy near the cutoff wave number k_c.

The effective viscosity ν_e, responsible for nonlocal interactions between wave numbers $k \ll k_c$ and $k \gg k_c$, is a function of some mean values representative of the actual state of turbulence. Chollet and Lesieur[3] relate ν_e to the value of $E(k_c)$ of the energy spectrum at the cutoff:

$$\nu_e = C_1 E(k_c)^{1/2} k_c^{-1/2} \tag{6}$$

Leslie and Quarini[10] relate ν_e to the value of $\langle S_{ij} S_{ij} \rangle$ obtained from the scalar $S_{ij} S_{ij}(\boldsymbol{k})$ of the Smagorinsky model, which has been averaged over all space,

$$\nu_e = (C_2 \Delta)^2 \langle 2 S_{ij} S_{ij} \rangle^{1/2} \tag{7}$$

The author has tried to incorporate in ν_e a "natural" dependence on k by taking not the mean of $S_{ij} S_{ij}(\boldsymbol{k})$ over all space, but averages over spherical caps Ω_k, i.e., by taking the three-dimensional spectrum of $S_{ij} S_{ij}(\boldsymbol{k})$:

$$\nu_e = C_3 \Delta^{3/2} \langle 2 S_{ij} S_{ij}(k) \rangle_{\Omega_k}^{1/2} \tag{8}$$

These models are easy to implement. $E(k_c)$ or $\langle S_{ij} S_{ij} \rangle$ vary slowly and can be evaluated only every 10 or 20 time steps. There is no need for inverse Fourier transforms to the physical space as for the classical "local" Smagorinsky model, which has been widely utilized in LES, in particular by Kwak et al.[6] in the case treated herein.

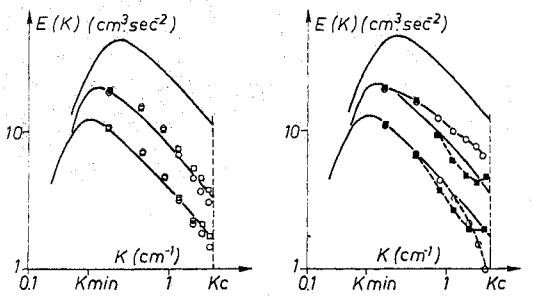

Fig. 1 Decaying isotropic turbulence; comparison of simulated spectra (16^3 simulation) with experiment.[4] a) ——— measured spectra; ○, model $\nu_T = \nu_e [1 + \lambda \times (K/K_c)^{2(\alpha-1)}]$, $\nu_e \sim E(K_c)^{1/2}$; □, model $\nu_e \sim \Delta^2 \langle S_{ij} S_{ij} \rangle^{1/2}$. b) ——— measured spectra; ○, model $\nu_T = C^{te} [1 + \lambda \times (K/K_c)^{2(\alpha-1)}]$; ■, model $\nu_T = C^{te} \cdot E(K_c)^{1/2} K_c^{-1/2}$.

Table 1 Eddy-viscosity subgrid-scale models

I	$\nu_T(k,k_c) = \nu_e F(k/k_c)$
II	$F(k/k_c) = 1 + \lambda (k/k_c)^{2(\alpha-1)}$
III	$\nu_e = C_1 E(k_c)^{1/2} k_c^{-1/2}$
IV	$\nu_e = (C_2 \Delta)^2 \langle 2 S_{ij} S_{ij} \rangle^{1/2}$
V	$\nu_e = C_3 \Delta^{3/2} \langle 2 S_{ij} S_{ij}(k) \rangle_{\Omega_k}^{1/2}$
	Δ = mesh size of computational grid
	k_c = cutoff wave number

Table 2 Constants of subgrid-scale models

II	$\lambda = 1.15$, $\alpha = 5$
III	$C_1 = 0.267$
IV	$C_2 = 0.275$
	$\Delta = 1.5$ cm
	$k_c = 2.096\ \text{cm}^{-1}$; $k_{\min} = 0.262\ \text{cm}^{-1}$

Energy spectra obtained (Fig. 1a) compare well with the data of Comte-Bellot and Corrsin[4] at the two measurement stations ($U_t/M=98$ and 171 with $U=10$ m/s and $M=5.08$ cm). Adjustment constants used (in 16^3 simulations with a computational mesh $\Delta=1.5$ cm) are listed in Table 2. Results obtained with Eq. (8) (not reported) are similar.

Spectra displayed on Fig. 1b show the necessity of the two requirements fulfilled by the previous models:

1) ν_e must vary with the state of the turbulence. If it is assumed to be a constant, incorrect spectra are obtained (open symbols); in the case shown, the constant value of ν_e is too low at the beginning of the decay and too high at the final stage.

2) $F(k/k_c)$ must have a sufficiently large value near the cutoff (at least with the sharp filter used). If it is assumed to be a constant, energy accumulates at the cutoff (closed symbols), because of insufficient drain toward the subgrid scales.

Several runs done with Eq. (8) and $F(k/k_c)=1$ show that, although $\langle S_{ij}S_{ij}(k)\rangle_{\Omega_k}^{1/2}$ increases with k, this increase is not sufficient in itself (in the 16^3 case) to insure the correct energy transfer at k_c.

In the following, results shown with 16^3 LES have been obtained with Eqs. (5) and (6). The other formulations give essentially similar results.

B. "Anisotropic" Computational Grid

In order to perform accurate simulations of homogeneous turbulence submitted to plane strains, the initial computational box must be predistorted to achieve the experimental range of variation of the dimensionless parameter Dt (product of strain rate D by time t). Attention must be given then, to the anisotropic distribution of computing points and to the degree of stretching of computing meshes.

1) The anisotropic distribution of the computing points induces errors in computed three-dimensional spectra $E_{ii}(k)$ of the velocity components $\hat{u}_i(\boldsymbol{k})$, resulting in oscillations particularly visible in the 16^3 simulations for a rectangular predistorted box (see Fig. 2). This geometric effect can be corrected as shown in Fig. 2 for $E_{22}(k)$; explicit correction formulas are given in the Appendix. The differences subsisting between the spectrum computed in the cubic box and the corrected spectrum computed in the rectangular box (Fig. 2) can be attributed to the second effect discussed thereafter.

2) Roy[17] has shown in the case of two-dimensional shear,[14] that, for stretching ratio $\Delta k_{max}/\Delta k_{min}\geq 2$, the loss of resolution in the direction of stretching induces errors for the smallest scales of turbulence. In the present case, this leads to an artificial anisotropy of the turbulence, especially in the 16^3 case, as evidenced by simulations performed with differently stretched rectangular boxes. These results have urged the author to look for some more favorable geometric configurations to lower the stretching ratio of the "rectangular" grid.

This can be achieved by rotating the initial cubic box of an angle α_0 around the K_1 axis before predistorting it. The case $q_0=j/4$ results in a "diamond-shaped" box, whose stretching ratio ($Rk_{max}/Rk_{min}\frac{7}{8}1.46$) is much more favorable than that of the rectangular box ($\Delta k_{max}/\Delta k_{min}\approx 4$). This leads to a spectacular improvement of the quality of the energy spectra, as shown in Fig. 3 for the 64^3 FTS case.

The anisotropy which appears in Fig. 3a for $K\geq 10$ is due essentially to the stretching of the rectangular computing grid. The anistrophy appearing in Fig. 3b for $K\geq 20$ comes from the geometric anisotropy of the grid and could be corrected as noted previously.

For completeness, the spectra obtained with an "isotropic" grid are shown in Fig. 3c. The difference between the energy spectra of Figs. 3b and 3c, for $K\geq 20$, is due to the fact that these spectra are not yet normalized by the number of computing points lying within each spherical cap centered on K.

The geometries which will be used when distorting the computational grids by two successive plane strains with an angle α between them are sketched on Fig. 4. (See Fig. 5 for a definition of the angle α.)

Three particular geometries are displayed corresponding to $\alpha_0=0$, $\pi/4$, and $\pi/8$. The effects of the successive deformations on the initial geometries (a) are sketched, after the first deformation (b), and after the second deformation, for two particular values of α: $\alpha=0$ (c), and $\alpha=\pi/4$ (d).

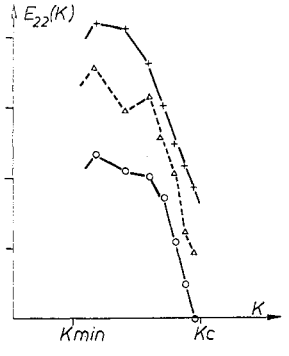

Fig. 2 Decaying isotropic turbulence; influence of the distortion of the computational box on the computed spectra $E_{ii}(K)$ (16^3 simulation). +, cubic box; △, rectangular box; ○, rectangular box, spectrum corrected by Eq. (A8).

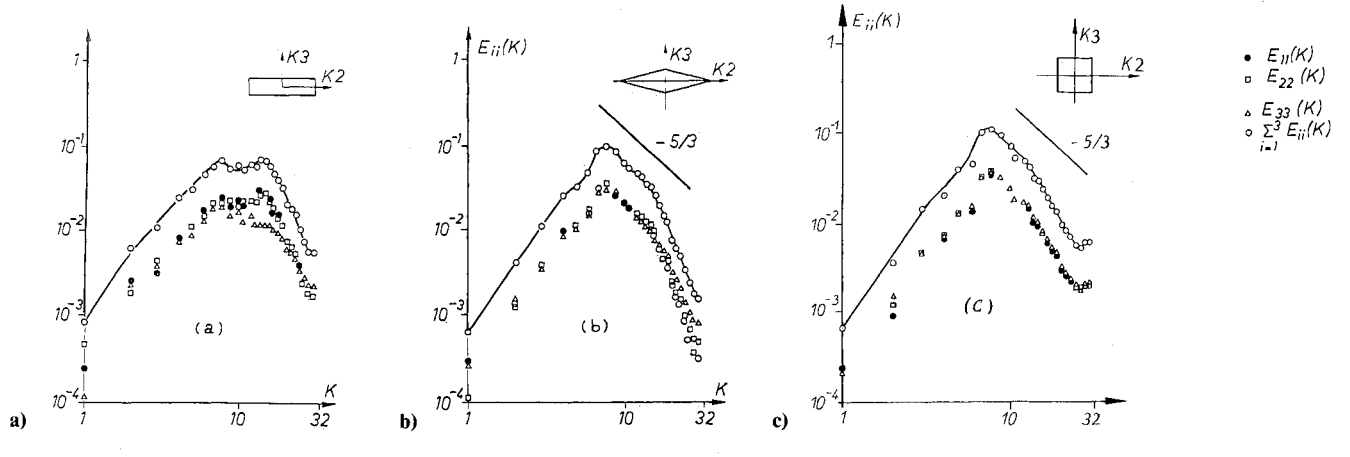

Fig. 3 Decaying isotropic turbulence; effect of geometries of the computational box on three-dimensional spectra (64^3 simulation). a) rectangular box; b) diamond-shaped box; c) cubic box.

The simulations described thereafter are achieved with the initial geometry corresponding to $\alpha_0 = \pi/4$. In this case, if $\alpha = \pi/4$, the final geometry is a rectangle, as can be seen in Fig. 4d. To avoid it one can use the initial geometry defined by $\alpha_0 = \pi/8$.

In Sec. III.C, comparisons are made between results obtained by LES with these two initial configurations.

III. Simulations of Homogeneous Turbulence Submitted to Two Successive Plane Strains

A. Gence's Experiment

64^3 FTS and 16^3 LES have been carried out for the experiment performed by Gence[5]: initially isotropic turbulence is submitted to two successive plane strains perpendicular to the mean flow direction (see Fig. 5, axis 1). Principal axes of the first deformation (2,3) and principal axes of the second deformation (2′,3′) differ by an angle α. Due to the presence of the second deformation, two interesting new phenomena have been pointed out:

1) In the case $\alpha = \pi/2$ where the two deformations are opposed, the turbulence anisotropy resulting from the first deformation is cancelled by the second one. Therefore, due to a certain "memory" of the turbulence, there is a return to isotropy in the presence of a deformation.

2) In the cases $0 < \alpha < \pi/2$ where the two deformations have their principal axes "not aligned", the principal axes (II, III) of the Reynolds stress tensor $\langle u_i u_j \rangle$, originally aligned with (2,3), rotate during the second deformation to realign with the axes (2′,3′). Thus, this experiment appears to be an interesting first step for testing codes and models, before handling more complex flows including rotation.

B. 64^3 Full-Turbulence Simulations

These 64^3 simulations have been performed with the collaboration of Roy. The Reynolds number simulated is equivalent to those of Rogallo's plane strain simulations:

$$R_\lambda = \sqrt{\overline{q^2}}\,\lambda/\nu \approx 25 \tag{9}$$

A diamond-shaped ($\alpha_0 = \pi/4$) initial box has been used to lower the stretching ratio of the computational grid as discussed in Sec. II.B. An isotropic simulation was first carried out in this predistorted box to obtain a developed isotropic field as the initial condition for the first deformation (see spectra of Fig. 3). The value of the strain rate D ($D = 4$) was chosen so that the ratio τ_D/τ_Q of characteristic times τ_D and τ_Q approximately equals the experimental value of 0.7. The time $\tau_D = 1/D$ is characteristic of the deformation rate and $\tau_Q = \overline{q^2}/2\epsilon_0$ is characteristic of the turbulence decay.

The experimental initial value of the dissipation rate ϵ_0 has been roughly estimated to 5.5 $m^2\ s^{-3}$ by equating $-2\epsilon_0$ to the estimated value of the initial slope $(d\overline{q^2}/dt)_0$ of the energy decay.

Figure 6 displays the time evolutions of the turbulence energy $\overline{q^2}$ nondimensionalized by its initial value $\overline{q_0^2}$. The comparison with experiment shows that, during the second deformation, the simulated decreases of energy are more pronounced than the experimental ones.

Several reasons can be invoked to explain these discrepancies, albeit no firm conclusion can be given at present. The reasons are as follows:

1) The low Reynolds number of the simulations.

2) Differences in anisotropy characteristics between the simulated and experimental initial fields ($II \approx 7 \times 10^{-5}$, $III < 0$ for the simulated field and $II \approx 1.5 \times 10^{-2}$, $III > 0$ for the experimental field); the simulated initial field being much more isotropic.

3) The presence of inhomogeneity in the experimental flow which was not taken into account in the simulations.

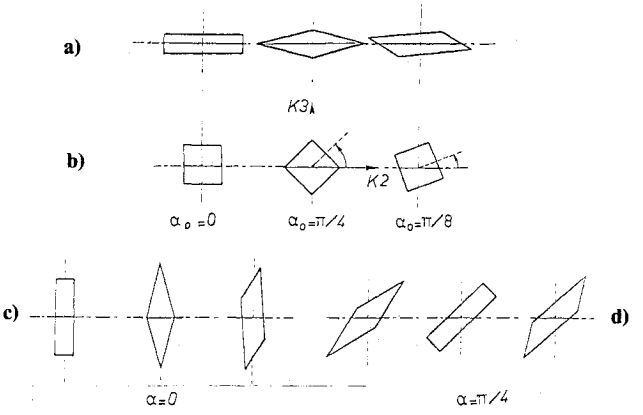

Fig. 4 Simulation of Gence's experiment; geometric configurations after each deformation, for three different initial configurations corresponding to $\alpha_0 = 0$, $\pi/4$, and $\pi/8$: a) initial geometric configurations; b) after the first deformation, c) after the second deformation, with an angle $\alpha = 0$ between the two deformations; d) after the second deformation, with an angle $\alpha = \pi/4$ between the two deformations.

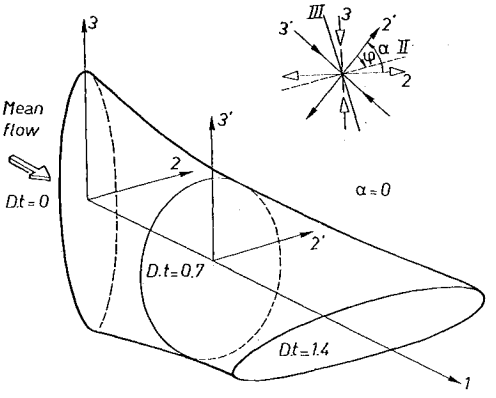

Fig. 5 Coordinates in Gence's experiment.

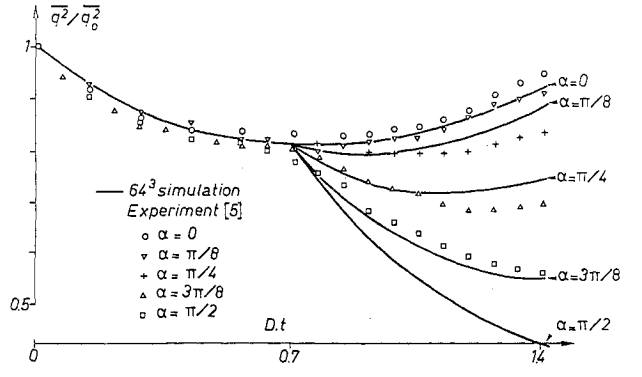

Fig. 6 64^3 FTS time evolutions of turbulence energy. ——— 64^3 simulation; o, ▽, +, △, □, experiments.[5] o, $\alpha = 0$; ▽, $\alpha = \pi/8$; +, $\alpha = \pi/4$; △, $\alpha = 3\pi/8$; □, $\alpha = \pi/2$.

Note that the experimental evolution of energy is not unique during the first deformation, and that it varies with the angle α.

Figure 7 displays the time evolution of parameter K [computed in the frame (II, III)]:

$$K = (\overline{u_{III}^2} - \overline{u_{II}^2})/(\overline{u_{II}^2} + \overline{u_{II}^2}) \tag{10}$$

the most sensitive parameter, characteristic of the anisotropy of the field.

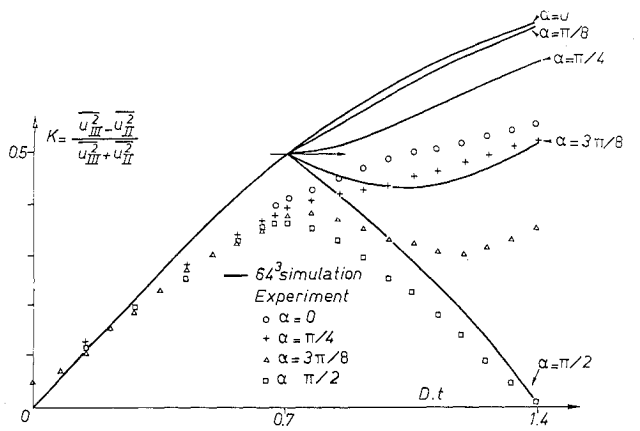

Fig. 7 64^3 FTS time evolutions of turbulence anisotropy (see Fig. 6 for legend).

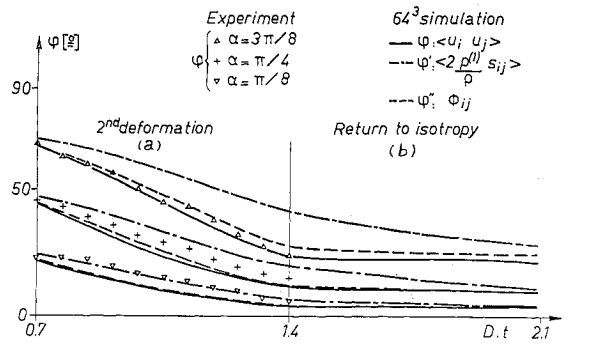

Fig. 8 64^3 FTS reorientation process of the tensors. a) second deformation; b) return to isotropy. 64^3 simulation: ——— angle φ between the principal axes of $\langle u_i u_j \rangle$ and those of the new deformation, $-\cdot-$ angle φ' corresponding to the tensor $\langle 2(p^{(1)}/\rho)S_{ij}\rangle$; - - - angle φ'' corresponding to the tensor ϕ_{ij}. Experiment: △, +, ▽, angle φ; △, $\alpha=3\pi/8$; +, $\alpha=\pi/4$; ▽, $\alpha=\pi/8$.

Comparison with experiment shows that the final simulated field is more anisotropic than the experimental one, except for $\alpha=\pi/2$. Nevertheless, the experimental trends are qualitatively well recovered and the important physical phenomena are well reproduced.

In particular, for $\alpha=\pi/2$ (where the two successive strains act in opposite directions), turbulence energy is transferred back to the mean flow, so that there is a return to isotropy in the presence of strain. This is well described by the simulation; the evolution of the anisotropy is quasisymmetrical during the two deformations (see Fig. 7). For $\alpha=\pi/4$ it has been shown,[5] with some simplifying assumptions, that the initial slope $(dK/dt)_0$ is equal to zero at the beginning of the second deformation. This is verified better by the simulated values than by the experimental ones.

Figure 8 describes the reorientation process of the Reynolds stress tensor during the second deformation. The experimental evolutions of angle φ between the principal axes of $\langle u_i u_j \rangle$ and those of the new deformation are well recovered by the simulation. As is evident in the experimental results, the stress tensor ceases to rotate after the second strain has been suppressed. Moreover, the reorientation process of the slow-pressure strain tensor $\langle (p^{(1)}/\rho)S_{ij}\rangle$, not accessible by experiment, can be described (angle φ' in Fig. 8). This tensor is not "aligned" with the Reynolds stress tensor, its reorientation is slower, and it goes on rotating after the second deformation has been suppressed.

More interesting is the reorientation process of the tensor ϕ_{ij} (angle φ'' in Fig. 8) defined by

$$\phi_{ij} = -\frac{\langle 2(p^{(1)}/\rho)S_{ij}\rangle}{\epsilon} + \frac{\epsilon_{ij} - \frac{2}{3}\epsilon\delta_{ij}}{\epsilon} \qquad (11)$$

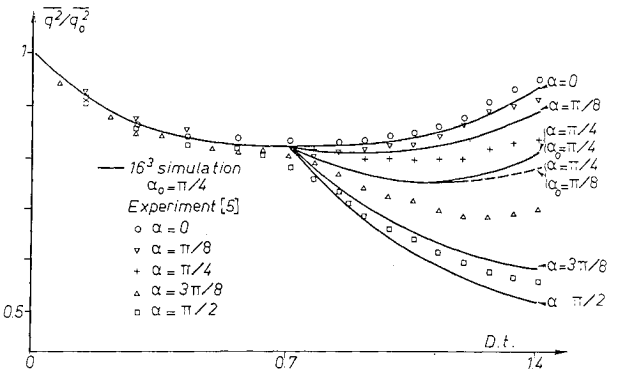

Fig. 9 16^3 LES time evolutions of turbulence energy. ——— 16^3 LES with initial box defined by $\alpha_0=\pi/4$, - - - 16^3 LES with initial box defined by $\alpha_0=\pi/8$, ○, ▽, +, △, □ experiment (see Fig. 6 for legend).

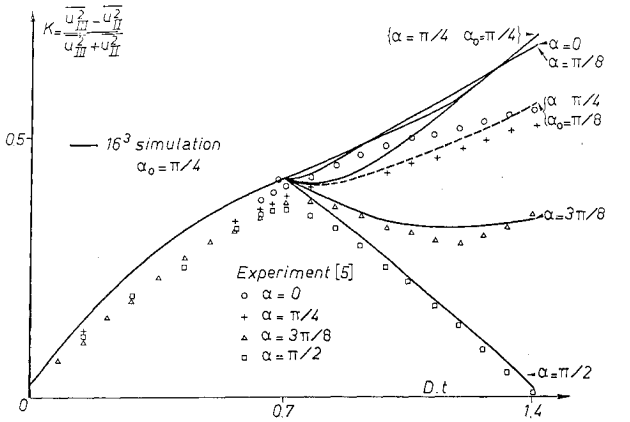

Fig. 10 16^3 LES time evolutions of turbulence anisotropy (see Fig. 9 for legend).

The simulation shows that ϕ_{ij} is "aligned" with $\langle u_i u_j \rangle$ ($\varphi \approx \varphi''$ in Fig. 8), so that ϕ_{ij} can be related linearly to the anisotropy tensor b_{ij}, as suggested by Lumley and Newman[11]:

$$\phi_{ij} = \beta b_{ij}; \qquad b_{ij} = \frac{\langle u_i u_j \rangle}{\langle u_k u_k \rangle} - \frac{\delta_{ij}}{3} \qquad (12)$$

The approximate values $1.5 \leq \beta \leq 3$ deduced from the present simulation at $Re \leq 10$ are consistent with Lumley's predictions and Rogallo's results for the relaxation from axisymmetric strain.

C. 16^3 Large Eddy Simulations

In the case of a computational box varying with time under the action of strains, the eddy viscosity must become anisotropic and adapt itself to the distortion of the box.

Equations (4-6) retained for ν_T are adapted to the anisotropic case as follows. The values of $F(k/k_c)$ are computed according to Eq. (5) at points (k_i) of the reference frame and used for the computations carried at points (k_i') of the moving frame, related to (k_i) by means of the following transformation:

$$k_i' = B_{ji}^{-1} k_j \qquad (13)$$

equivalent to Eq. (1).

The effective viscosity ν_e defined by Eq. (6) has been split in the three stretching directions and energies $E(k_{ic})$ at cutoff wave number k_{ic} in the direction i have been computed for points located near the boundaries of the box.

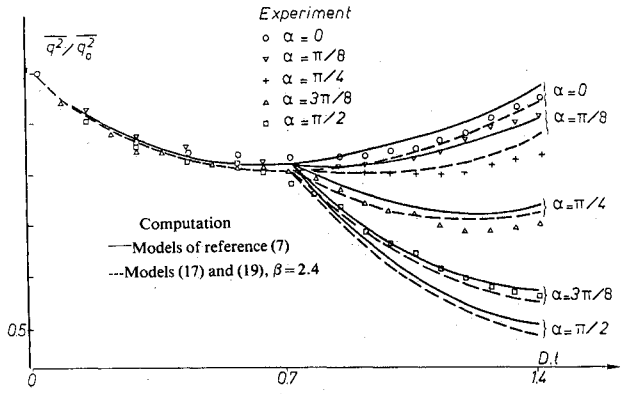

Fig. 11 Results of one-point closure models, time evolutions of turbulence energy. ——— models of Ref. 7; - - - Eqs. (17) and (19), with $\beta = 2.4$. ○, ▽, +, △, □ experiment (see Fig. 6 for legend).

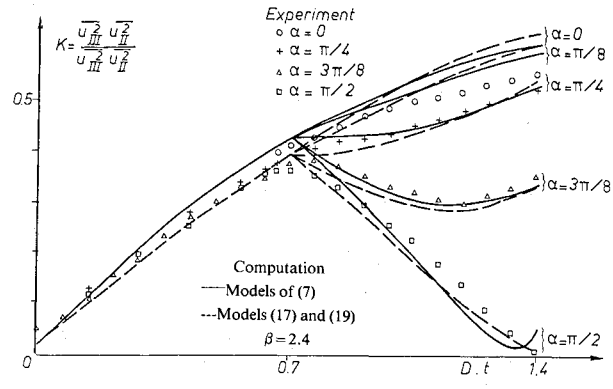

Fig. 12 Results of one-point closure models, time evolutions of turbulence anisotropy (see Fig. 11 for legend).

Constants of models are the same as those used in the isotropic case.

Simulated time evolutions of energy and anisotropy are displayed in Figs. 9 and 10. The initial predistorted box is a diamond-shaped one ($\alpha_0 = \pi/4$). As pointed out in Sec. II.B, this leads to a final rectangular box in the case $\alpha = \pi/4$ (see Fig. 4). Results obtained in this particular case for parameter K (Fig. 10) show an abnormal enhancement of the anisotropy of the turbulence. The same computations carried out again with $\alpha_0 = \pi/8$ gives a more satisfying time evolution of K (dashed line).

Results obtained for the reorientation process of the three tensors, discussed in Sec. III.B (angles φ, φ', and φ''), are similar to those of the 64^3 FTS, and are not shown here.

D. Application to One-Point Closure Models

One important aim of numerical simulations is to devise better models for the unknown terms of the Reynolds stress equations, specially those difficult to measure experimentally.

Classical models for the dissipation and pressure/strain terms[7] are as follows in the case of high Reynolds number flows:

$$\epsilon_{ij} = \tfrac{2}{3}\epsilon\delta_{ij} \tag{14}$$

$$\left\langle 2\frac{p^{(1)}}{\rho} S_{ij} \right\rangle = -2C_1 b_{ij}\epsilon \tag{15}$$

$$\left\langle 2\frac{p^{(2)}}{\rho} S_{ij} \right\rangle = -\frac{C_2+8}{11}(P_{ij} - \tfrac{2}{3}P\delta_{ij}) + \ldots \tag{16}$$

where P_{ij} is the production of $\langle u_i u_j \rangle$ and P the production of $\langle u_k u_k \rangle$. C_1 and C_2 are constants.

The Rotta[16] hypotheses (14) and (15) are not consistent with the results obtained by the simulations at low Reynolds number:

$$\epsilon_{ij} - \tfrac{2}{3}\epsilon\delta_{ij} \neq 0 \tag{17}$$

$$\langle 2(p^{(1)}/\rho)S_{ij} \rangle - (\epsilon_{ij} - \tfrac{2}{3}\epsilon\delta_{ij}) = -\phi_{ij}\epsilon = -\beta b_{ij}\epsilon$$

From a practical point of view, these two formulations are strictly equivalent, with $\beta = 2C_1$.

However, it seems easier to describe the influence of the Reynolds number using Eq. (17) rather than Eq. (15). As shown in Ref. 15, β is a function of the Reynolds number.

Simulation results obtained for homogeneous shear[15] can be roughly approximated by

$$\beta \approx 2 + 0.6Re^{0.35} \qquad Re \leq 300 \tag{18}$$

In order to evaluate Eq. (17) at a higher Reynolds number, the differential equations have been solved for the Reynolds stresses and the dissipation rate ϵ in the homogeneous case by a fourth-order Runge-Kutta method.

First, the computations have been carried out with Eqs. (14-16) and constants prescribed by Launder et al.[7] ($C_1 = 1.5$, $C_2 = 5$).

The results are shown in Figs. 11 and 12 with solid lines. Experimental evolutions of energy and anisotropy are reasonably well recovered, and very similar to the simulation results.

Then, Eq. (17) has been tested with Eqs. (16) and (18), together with a relationship suggested by Reynolds,[14] relating the constant C_2 of Eq. (16) to the anisotropy parameter G:

$$C_2 = 10/7 - 24(1/9 - G) \tag{19}$$

with

$$G = 1/9 + \mathrm{III} - \mathrm{II}/2$$

Results obtained show that Eq. (18) deduced from the shear case is not valid in our case and a constant value $\beta = 2.4$ consistent with our simulation results has been adopted in the following. Dashed lines in Figs. 11 and 12 correspond to a computation carried out with Eqs. (17) and (19) and $\beta = 2.4$. Results are slightly better for K but no real improvement has been obtained.

IV. Conclusions

Simple eddy-viscosity subgrid-scale models have been evaluated in 16^3 LES of isotropic and anisotropic homogeneous turbulence.

The formulation adopted for the eddy viscosity insure both a strong local energy transfer near the cutoff wave number and a time-dependent nonlocal transfer. They were shown to work satisfactorily in the case of plane strains.

These models will enable us to simulate higher Reynolds number flows at very low cost when they are incorporated in the 64^3 simulation code running on a parallel computing system.

Practical solutions have been proposed to minimize numerical difficulties arising from the use of stretched computational grids.

In the case of Gence's experiment, 16^3 LES and 64^3 FTS were able to capture the physics of turbulence evidenced by the experiment and have given more detailed information on the pressure mechanisms. However, no practical information can be deduced as yet from these results because of the low Reynolds number of the simulations.

Appendix: Correction Formula for the Computation of Spectra $E_{ii}(k)$ in the Case of Distorted Computational Grids

Three-dimensional spectra $E_{ii}(k)$ are computed according

$$E_{ii}(k) = \frac{4\pi K^2 \Delta K}{N_K} \sum_{\Omega_k} \hat{u}_i^2(\boldsymbol{K}'); \quad i=1,2,3 \tag{A1}$$

where the sum Σ is taken over the N_k vectors $\boldsymbol{k}'$ whose extremities lie within a spherical cap of volume $\Delta\Omega_k = 4\pi k^2 \Delta K$ centered on k:

$$k' \epsilon \left[k - \frac{\Delta K}{2},\ k + \frac{\Delta K}{2} \right] \tag{A2}$$

The three-dimensional energy spectrum is defined by

$$E(k) = \tfrac{1}{2}\left[E_{11}(k) + E_{22}(k) + E_{33}(k) \right] \tag{A3}$$

According to the incompressibility condition, the velocity vector lies within the plane perpendicular to $\boldsymbol{k}'$ and can be expressed by means of two orthogonal unit vectors $\boldsymbol{a}$ and $\boldsymbol{b}$:

$$\boldsymbol{a} \equiv \left(-\frac{\sqrt{k'^2 - k_1'^2}}{k'};\ \frac{k_1' k_2'}{k'\sqrt{k'^2 - k_1'^2}};\ \frac{k_1' k_3'}{k'\sqrt{k'^2 - k_1'^2}} \right)$$

$$\boldsymbol{b} \equiv \left(0;\ \frac{k_3'}{\sqrt{k'^2 - k_1'^2}};\ -\frac{k_2'}{\sqrt{k'^2 - k_1'^2}} \right) \tag{A4}$$

So that, in the local frame $(\boldsymbol{k}', \boldsymbol{a}, \boldsymbol{b})$,

$$\hat{\boldsymbol{u}}(\boldsymbol{k}', \theta) = \boldsymbol{a}\cos\theta + \boldsymbol{b}\sin\theta; \quad \theta \epsilon [0, 2\pi] \tag{A5}$$

In the case of a random velocity fied $\hat{v}$, with a constant probability density function (equal to one)

$$\hat{v}_i^2(\boldsymbol{k}') = \int_0^{2\pi} \hat{v}_i^2(\boldsymbol{k}', \theta)\, d\theta = \pi \left(1 - \frac{k_i'^2}{k'^2} \right) \tag{A6}$$

Three-dimensional spectra $F_{ii}(k)$ or $\hat{v}_i^2$ depend explicitly on the geometric distribution of the points in spectral space.

$$F_{ii}(k) = \frac{4\pi K^2 \Delta K}{N_K} \sum_{\Omega_k} \pi \left(1 - \frac{k_i'^2}{k'^2} \right) \tag{A7}$$

For isotropic turbulence, $F_{ii}(k)$ must be identical for $i=1,2,3$. This is not the case if the computational grid is distorted and the geometric distribution of points is anisotropic. The energy spectrum

$$F(k) = \frac{1}{2} \sum_{i=1}^{3} F_{ii}(k)$$

is not affected.

One can define a correction coefficient by

$$\eta(k) = \underset{\text{isotropic}}{F_{ii}(k)} / \underset{\text{anisotropic grid}}{F_{ii}(k)} \tag{A8}$$

and spectra $E_{ii}(k)$ can be corrected by:

$$\underset{\text{corrected}}{E_{ii}(k)} = \underset{\text{uncorrected}}{E_{ii}(k)} \times \eta(k)$$

Acknowledgments

The author expresses his gratitude to Y. F. Morchoisne for his helpful suggestions during the course of this study, and wishes to acknowledge the substantial contributions made by Ph. Roy and P. Leca to this work. The author also wishes to thank C. Basdevant and R. Sadourny for helpful discussions.

References

[1] Bardina, J., Ferziger, J. H., and Reynolds, W. C., "Improved Subgrid-Scale Models for Large Eddy Simulation," AIAA Paper 80-1357, 1980.

[2] Basdevant, C., Lesieur, M., and Sadourny, R., "Subgrid-Scale Modeling of Enstrophy Transfer in Two-Dimensional Turbulence," *Journal of Atmospheric Sciences*, Vol. 35, 1978, pp. 1028-1042.

[3] Chollet, J. P. and Lesieur, M., "Parameterization of Small Scales of Three-Dimensional Isotropic Turbulence Utilizing Spectral Closures," *Journal of Atmospheric Sciences*, Vol. 38, 1981, pp. 2747-2757.

[4] Comte-Bellot, G. and Corrsin, S., "Simple Eulerian Time Correlation of Full- and Narrow-Band Velocity Signals in Grid Generated Isotropic Turbulence," *Journal of Fluid Mechanics*, Vol. 48, 1971, p. 273.

[5] Gence, J. N., "Action de deux déformations pures planes successives sur une turbulence isotrope," These de Doctorat d'Etat, Université Claude Bernard, Lyon, France, 1979.

[6] Kwak, D., Reynolds, W. C., and Ferziger, J. H., "Three-Dimensional Time Dependent Computation of Turbulent Flow," Mechanical Engineering Department, Stanford University, Stanford, Calif., Rept. TF-S, 1975.

[7] Launder, B. E., von Kármán Institute, Rhode-Saint-Genese, Belgium, Lecture Series, 1980-3, 1980.

[8] Leca, P. and Roy, Ph., "Numerical Simulation on a Multiprocessor System," *Proceedings of the 1st International Colloquium on Vector and Parallel Computing in Scientific Applications*, Paris, March 1983, pp. 95-101.

[9] Leonard, A., "Energy Cascade in Large-Eddy Simulations of Turbulent Fluid Flows," *Advances in Geophysics*, Vol. A18, 1974, pp. 237-248.

[10] Leslie, D. C. and Quarini, G. L., "Application of Turbulence Theory to the Formulation of Subgrid Modeling Procedures," *Journal of Fluid Mechanics*, Vol. 91, 1979, pp. 65-91.

[11] Lumley, J. L. and Newman, G. R., "The Return to Isotropy of Homogeneous Turbulence," *Journal of Fluid Mechanics*, Vol. 82, 1977, pp. 161-178.

[12] Morchoisne, Y. F., "Pseudo Spectral Space-Time Calculations of Incompressible Viscous Flows," AIAA Paper 81-0109, 1981.

[13] Orszag, S. A. and Patterson, G. S., "Numerical Simulation of the Three-Dimensional Homogeneous Isotropic Turbulence," *Physical Review Letters*, Vol. 28, No. 2, 1972, p. 76.

[14] Reynolds, W. C., "Modélisation de la Turbulence," Ecole d'Eté Electricité de France d'Analyse Numérique Bréau sans Nappe, France, 1982.

[15] Rogallo, R. S., "Numerical Experiments in Homogeneous Turbulence," NASA TM 81315, 1981.

[16] Rotta, J. C., "Statistische theorie nichthomogener turbulenz," *Zeitschrift fuer Physik*, Vol. 129, 1951, pp. 547-572.

[17] Roy, Ph., "Numerical Simulation of Homogeneous Anisotropic Turbulence," *Proceedings of the 8th International Conference on Numerical Methods in Fluid Dynamics*, Aix-la-Chapelle, France, 1982, p. 440.

[18] Roy, Ph., "Résolution des Equations de Navier-Stokes par un schéma de haute précision en Espace et en Temps," *La Recherche Aérospatiale*, No. 6, 1980, p. 373.